International Journal of Geo-Information

MDPI

Article

Spatial and Temporal Evolution of the Infiltration Characteristics of a Loess Landslide

Dongdong Yang [1,2], Haijun Qiu [1,2,3,*], Yanqian Pei [1], Sheng Hu [1,2,3], Shuyue Ma [1], Zijing Liu [1], Yan Zhang [1] and Mingming Cao [1]

[1] College of Urban and Environmental Sciences, Northwest University, Xi'an 710127, China; yangdongdong@stumail.nwu.edu.cn (D.Y.); 201620795@stumail.nwu.edu.cn (Y.P.); shenghu@nwu.edu.cn (S.H.); msynwu@stumail.nwu.edu.cn (S.M.); liuzijing@stumail.nwu.edu.cn (Z.L.); 201731725@stumail.nwu.edu.cn (Y.Z.); chengshi@nwu.edu.cn (M.C.)

[2] Institute of Earth Surface System and Hazards, Northwest University, Xi'an 710127, China

[3] Shaanxi Key Laboratory of Earth Surface System and Environmental Carrying Capacity, Northwest University, Xi'an 710127, China

* Correspondence: haijunqiu@nwu.edu.cn; Tel.: +86-139-9134-5616

Received: 11 November 2019; Accepted: 18 December 2019; Published: 2 January 2020

Abstract: Infiltration plays an important role in influencing slope stability. However, the influences of slope failure on infiltration and the evolution of infiltration over time and space remain unclear. We studied and compared the infiltration rates in undisturbed loess and disturbed loess in different years and at different sites on loess landslide bodies. The results showed that the average initial infiltration rate in a new landslide body (triggered on 11 October 2017) were dramatically higher than those in a previous landslide body (triggered on 17 September 2011) and that the infiltration rates of both landslide types were higher than the rate of undisturbed loess. The initial infiltration rate in the new landslide body sharply decreased over the 4–5 months following the landslide because of the appearance of physical crusts. Our observations indicated that the infiltration rate of the disturbed soil in a landslide evolved over time and that the infiltration rate gradually approached that of undisturbed loess. Furthermore, in the undisturbed loess, both the initial and quasi-steady infiltration rates were slightly higher in the loess than in the paleosol, and in the previous landslide body, the infiltration rate was highest in the upper part, intermediate in the middle part, and lowest in the lower part. This study can help us to better understand the evolution process of infiltration in undisturbed loess, previous landslides, and new landslides.

Keywords: landslides; infiltration; loess; disturbed loess; physical crusts

1. Introduction

The infiltration and the strong collapsibility of loess are the main exogenic and endogenic factors, respectively, that contribute to loess landslides and the secondary failure of landslide bodies [1–6]. In recent years, loess-covered areas have been prone to rainfall-induced landslides due to variable climatic conditions and anthropogenic activities [7–9]. Moreover, large-scale landslide bodies tend to exhibit secondary failure due to an increased infiltration rate [10–12]. This phenomenon worsens the situation in landslide-prone areas.

The infiltration rate can be used to evaluate how quickly water enters the soil, and a high infiltration rate tends to greatly decrease the shear strength of the soil due to increases in the water content and pore water pressure [13–17]. Loess is characterized by well-developed vertical jointing and strong collapsibility, which significantly influence the infiltration process [3,18]. The collapsibility of loess tends to worsen due to the destruction of the soil structure during the landslide process, triggering

further secondary failures of the landslide body. According to statistical studies, 94.2% of landslides are associated with rainfall, and 5.6% of previous landslides were reactivated in the 2011–2016 period in the Chinese Loess Plateau [19–21].

Many studies have shown that loess slopes tend to fail due to their high infiltration capacity and collapsibility, especially under heavy rainfall or irrigation [9,16,20]. However, the infiltration process and the characteristics of the loess and the landslide body are extremely complex and are influenced by the physical properties, recovery state, crust, structure slope aspect, and gradient [22–25]. Several studies have focused on the infiltration characteristics, the failure mechanisms, and the triggering systems of loess landslides based on field monitoring of rainfall infiltration and laboratory experiments [1,15,26,27]. However, little attention has been paid to the spatial and temporal evolution of the infiltration characteristics in landslide bodies, especially in recent landslides. In fact, the variability and trends of infiltration in a landslide are extremely important factors for evaluating the stability of slopes and large-scale previous landslide bodies [22,28,29].

In this study, field investigations, infiltration experiments, and laboratory testing were conducted on undisturbed loess (UDL), a previous landslide body (PLB), and a new landslide body (NLB) associated with the Jiwachang Brickyard Landslide. Additionally, successive investigations and experiments were conducted on the NLB. According to the results, we try to explain how the infiltration characteristics changed with slope failure and how the infiltration evolved over time and space.

2. Study Area

The Bailu Loess Tableland (263 km^2) is located 5 km east of Xi'an city, Shaanxi Province, China (Figure 1a,b). The length and width are 28 km and 6–10 km, respectively. The stratigraphic unit comprises deposits of Malan loess, which was formed in the Late Pleistocene and is very sensitive to water because of its collapsibility [30], and Lishi loess, which was formed in the Middle Pleistocene and consists of interlayered loess and paleosol layers [3]. The Bailu Loess Tableland area has a semi-humid continental monsoon climate and is in the warm temperate zone, with a mean annual precipitation of 560 mm and a mean temperature of 13.1 °C [31]. The rainfall is mostly concentrated in the form of heavy precipitation in the summer and autumn, and the intensities vary from 1 mm/h to 20 mm/h. The Jiwachang Brickyard Landslide (34°16′00″ N, 109°05′49″ E) is located in the northwest corner of the Bailu Loess Tableland (Figure 1b). This landslide is characterized by a high speed and a long runout. The Jiwachang Brickyard Landslide was triggered on 17 September 2011 by heavy precipitation. In addition, the excavation of the brickyard contributed to this landslide to some extent, and this landslide destroyed the brickyard and killed 32 people [7]. The QR code (Figure 1g) shows a panorama of the Jiwachang Brickyard Landslide generated by an Unmanned Aerial Vehicle (UAV).

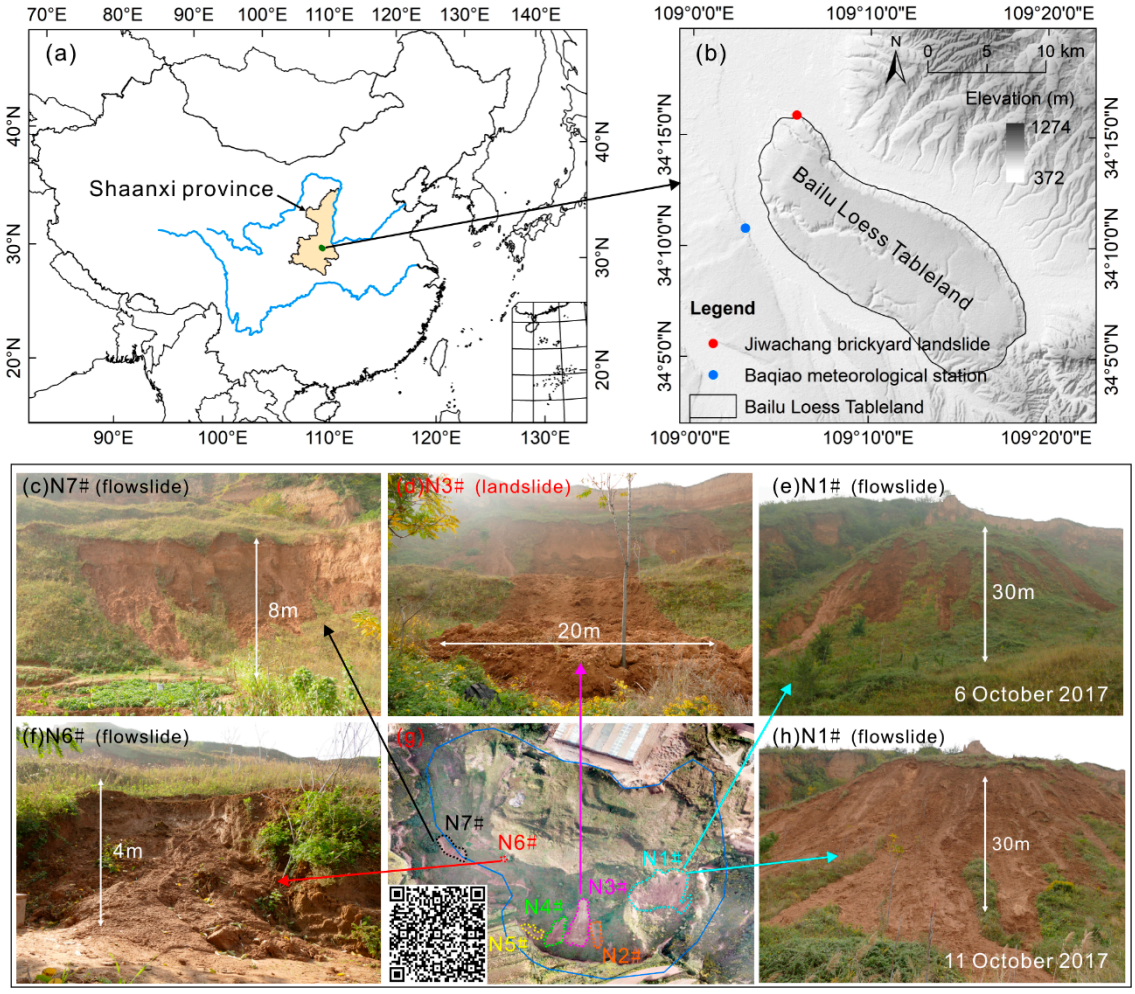

Figure 1. (**a**) Location of Shaanxi province, China. (**b**) Locations of the Jiwachang Brickyard landslide and Baqiao meteorological station. (**c**–**f**) and (**h**) show the new landslides and flowslides, and (**g**) shows the previous landslide body and location of three new landslides and four flowslides. The QR code shows a panorama of the Jiwachang Brickyard Landslide.

3. Field Investigation

Based on the field investigation, the typical landslide N3# was selected (hereinafter referred to as NLB) for the infiltration experiments. The characteristic parameters of the PLB, recent landslides and flowslides, were recorded during the investigation (Table 1, Figures 1c–h and 2). The sedimentary thicknesses of L1 (the first loess layer in the Malan loess), S1 (the first paleosol layer in the Lishi loess), and L2 (the first loess layer in the Lishi loess) are 8 m, 2 m, and 6 m, respectively. In total, approximately 90% of the PLB was covered by grass (Figure 2a), and biological crusts (Figure 2c), moss crusts (Figure 2d) and physical crusts were found to be abundant on the soil surface. However, grass and soil crusts were not observed on the NLB on 24 October 2017 (Figure 2b,e). The diameter of the fragmented loess blocks was 5–120 cm, but the diameter of most of the clods was less than 10 cm, which means that the structure of the soil in the NLB was severely disturbed.

Table 1. Parameters of the previous landslide, new landslides, and flowslides.

Type	Name	Relative Height Difference (m)	Length (m)	Distance (m)	Average Thickness (m)	Area (m^2)	Estimated Volume (m^3)	Triggered Date
Landslide	PLB	114	339	315	8	100,900	599,000	11 September 2011
Flowslide	N1#	30	50	80	0.5	4000	–	11 October 2017
Landslide	N2#	8	15	8	0.5	120	60	4–11 October 2017
Landslide	N3# (NLB)	12	70	15–25	0.8	1400	840–1400	11 October 2017
Landslide	N4#	9	22	12	0.6	270	162	4–11 October 2017
Flowslide	N5#	3	5	7	0.5	40	–	4–11 October 2017
Flowslide	N6#	4	8	8	1	70	–	4–11 October 2017
Flowslide	N7#	8	10	20	0.3	200	–	4–11 October 2017

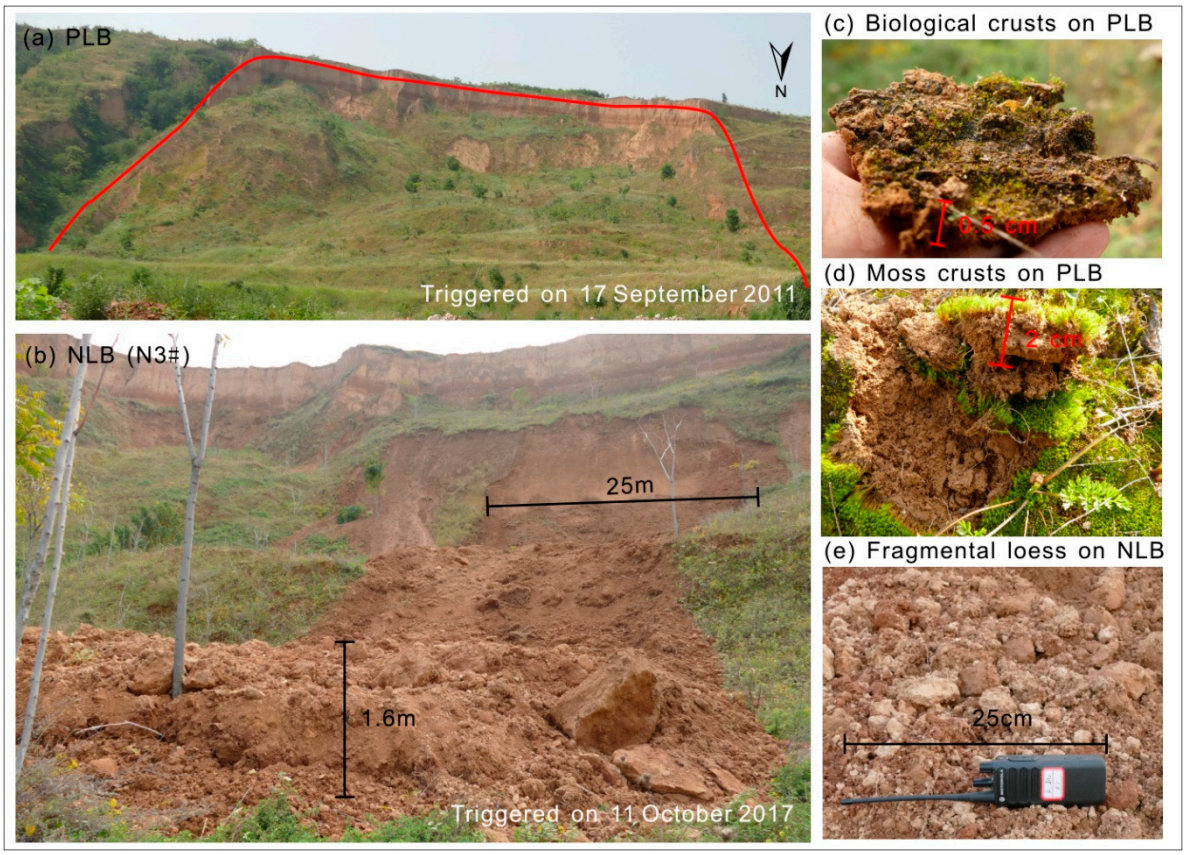

Figure 2. A view of the previous landslide body (PLB) and the new landslide body (NLB). (**a**) PLB, (**b**) NLB (N3#), (**c**) biological crusts on the PLB, (**d**) moss crusts on the PLB, and (**e**) fragmented loess on the NLB.

4. Materials and Methods

4.1. In Situ Infiltration Rate and the Physical Index Measurement

A single-cylinder permeameter (S-CP) (diameter of 4.8 cm, length of 10 cm) was used to measure the quasi-steady infiltration rate (QIR) and the initial infiltration rate (IIR) of the soil [13,32,33]. During the in-situ infiltration experiments, the vegetation was trimmed to the soil surface before inserting the S-CP, and animal burrows were avoided when choosing the experiment site. Several measurements may be needed to determine the QIR. The entire process required approximately 1–3 h for each experiment site. When the infiltration experiment was finished, 5 soil samples were collected by slowly pushing a core ring (dimension of 5 cm, volume of 100 cm^3) into the soil near the experiment site. The samples were then dried at 105 °C for 12 h in the laboratory and were used to measure the antecedent moisture content, bulk density, and porosity of the soil.

The IIR and QIR were calculated using the following equation [34]:

$$i = (\frac{VW}{t}) \times (1/\mathrm{A}) \quad (1)$$

where i is the IIR or QIR, VW is the volume of infiltrated water, t is the time required for the water to infiltrate, and A is the area of the cylinder ($\mathrm{A} = \pi r^2$, r = 2.4 cm).

The bulk density (g/cm^3) was calculated using the following equation [34]:

$$Bd = \frac{\rho}{1 + 0.01w} = \frac{\frac{m_0}{v}}{1 + 0.01w} \quad (2)$$

where Bd is the bulk density, ρ is the density of wet soil, m_0 is the weight of wet soil, v is the volume of the core ring (100 cm^3), and w is the moisture content (%).

The porosity (%) was calculated using the following equation [34]:

$$P = (1 - \frac{Bd}{\rho_d}) \times 100 \quad (3)$$

where P is the porosity, Bd is the bulk density, ρ_d is the specific gravity, as measured in the laboratory.

4.2. Experimental Design

To compare the differences in the infiltration rate among the UDL, PLB, and NLB, a series of experiments were conducted on 18 to 26 October 2017, in the L1, S1, and L2 soil layers (Figure 3a), the upper, middle, and lower parts of the PLB (Figure 3b), and the upper and lower parts of the NLB (Figure 3c). Flat surfaces were selected for the infiltration experiment, and the distances between the experimental points on the UDL, PLB, and NLB were 5 m, 50 m, and 5 m, respectively. It should be noted that the QIR of the NLB was difficult to measure during the experiment due to the strong collapsibility of the fragmented loess. Therefore, only the IIR of the soil was measured on the NLB. Successive infiltration experiments were conducted to identify changes in the infiltration rate in the NLB on 14 March 2018, and 17 July 2018.

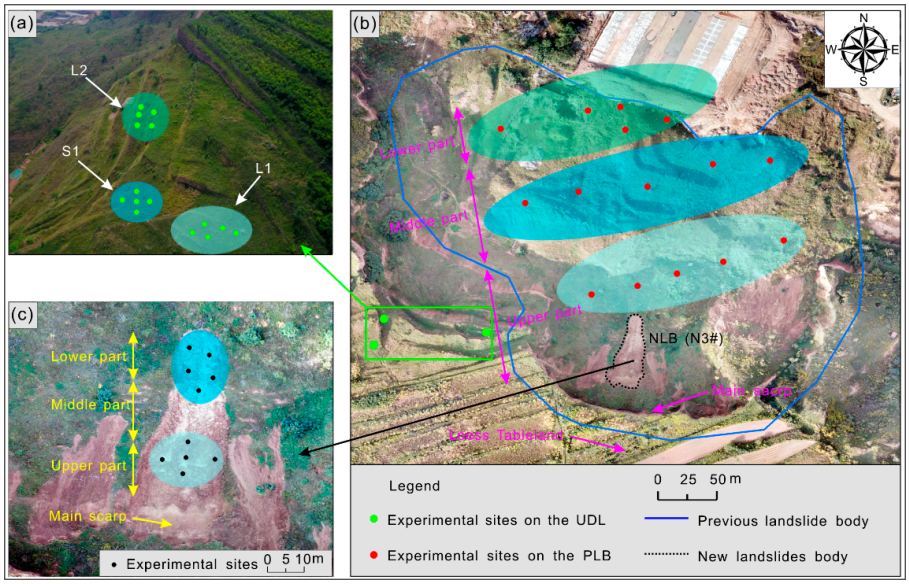

Figure 3. Schematic diagram of experimental infiltration sites for the undisturbed loess (UDL), previous landslide body (PLB) and new landslide body (NLB). Experimental infiltration sites on (**a**) the UDL, (**b**) the PLB, and (**c**) the NLB.

4.3. Statistical Analysis

The differences in the IIR, bulk density and porosity in the UDL, PLB, and NLB were evaluated with one-way ANOVA ($p < 0.05$) after testing for homogeneity of variance. The results in this study are expressed as the mean ± standard error of the mean (SEM). An independent t-test ($p < 0.05$) was used to evaluate the differences in the results of the infiltration experiments conducted on the NLB on 14 March 2018, and 17 July 2018. All statistical analyses were performed with SPSS 17.0 software (SPSS, Chicago, IL, USA).

5. Results

5.1. Occurrence of Landslides and Flowslides Associated with Precipitation

For the PLB, three recent landslides and four flowslides occurred in the Baqiao Brickyard because of the intense rainfall (Figure 1g). The antecedent (3 to 17 September 2011) accumulated precipitation reached 244.3 mm, and the daily precipitation was 40.2 mm (17 September 2011) (Figure 4a). The recent landslides and flowslides (Figure 1c–f,h) were triggered during the period from 4 to 11 October 2017, in the upper part of the PLB. The antecedent (23 September to 11 October 2017) accumulated precipitation reached 155 mm, and the daily precipitation was 30 mm (11 October 2017, time when landslide N3# was triggered) (Figure 4b), according to the Baqiao meteorological station. A small-scale flowslide occurred on 6 October 2017 (Figure 1e), but larger flowslides occurred on 11 October 2017 (Figure 1h), following heavy rainfall from 9 to 11 October 2017. Continuous precipitation was the main reason for the occurrence of several landslides and flowslides.

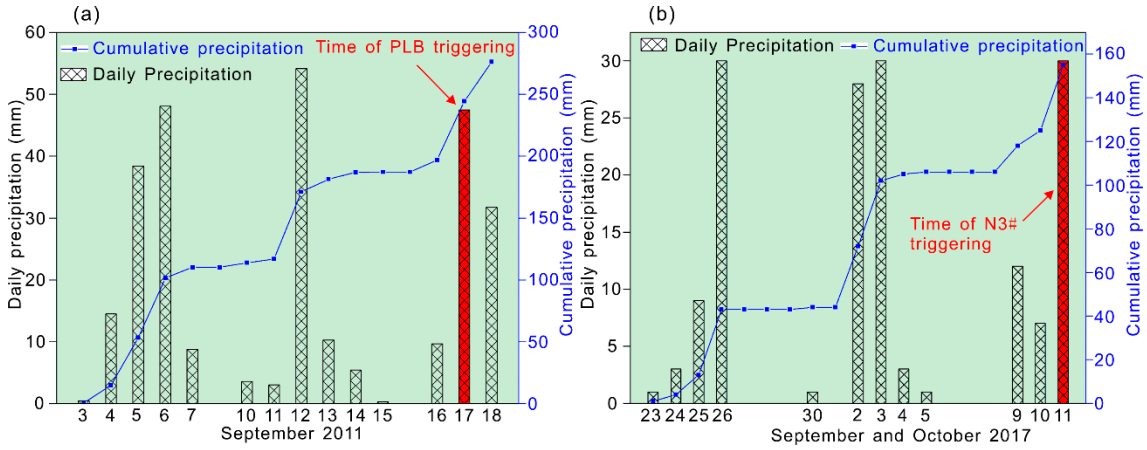

Figure 4. Distribution of daily and accumulated precipitation before the occurrences of the (**a**) previous landslide body (PLB) and (**b**) landslide N3# (data from the Baqiao meteorological station).

5.2. The Spatial Differences in Infiltration Characteristics across Sites

The different parts of the UDL, PLB, and NLB are characterized by large differences in the infiltration rates (Figure 5). In the UDL, the IIR was highest in soil layer L1 (mean ± SEM = 5.8 ± 0.9 mm/min), intermediate in soil layer L2 (4.9 ± 1.8 mm/min), and lowest in soil layer S1 (2.6 ± 0.7 mm/min) (Figure 5), but the differences were very small. In the PLB, the IIR was highest in the upper part (20.9 ± 4.0 mm/min), intermediate in the middle part (16.4 ± 5.2 mm/min), and lowest in the lower part (11.3 ± 3.8 mm/min) (Figure 5). In the NLB, the IIR was higher in the lower part (968.3 ± 68.1 mm/min) and lower in the upper part (742.6 ± 89.4 mm/min) (Figure 5). Furthermore, the QIR was highest in L1, intermediate in L2, and lowest in S1 (Figure 5) in the UDL. In the PLB, the QIR was highest in the upper part, intermediate in the middle part, and lowest in the lower part (Figure 5).

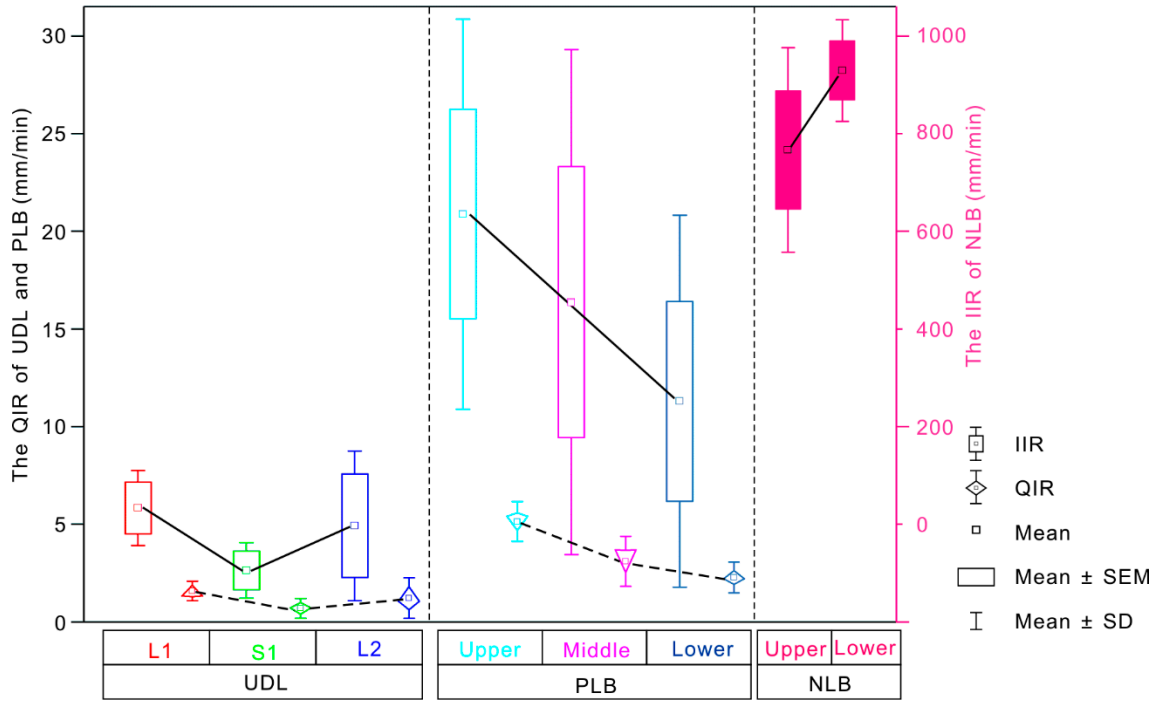

Figure 5. Spatial differences in the infiltration rate of the undisturbed loess (UDL), previous landslide body (PLB) and new landslide body (NLB). SEM is the standard error of mean. SD is the standard deviation.

Notably, the average IIR in the NLB was almost 200 times and 60 times higher than those in the UDL and PLB, respectively. Unsurprisingly, the rate at which water penetrated into the cracked soil was much higher than that into UDL and the seven-year-old landslide body. A comparison of the PLB and the UDL reveals a small but significant increase in the IIR, and the average IIR in the PLB was 4.4 times higher than that in the UDL ($p < 0.05$).

5.3. Physical Parameter Differences across Sites

Bulk density and porosity are the basic physical properties of soil. These properties have a direct influence on the soil infiltration properties and solute migration [35–38]. Based on the results generated for the UDL, PLB, and NLB (Figure 6), the UDL had the highest soil bulk density and the lowest porosity, while the NLB had the lowest soil bulk density and the highest porosity. The disturbed soils (PLB and NLB) exhibited a large and significant ($p < 0.05$) increase in porosity compared to the UDL (loess-paleosol sequences). Among the disturbed soils, there was a small and insignificant ($p = 0.074$) increase in the PLB compared with the NLB.

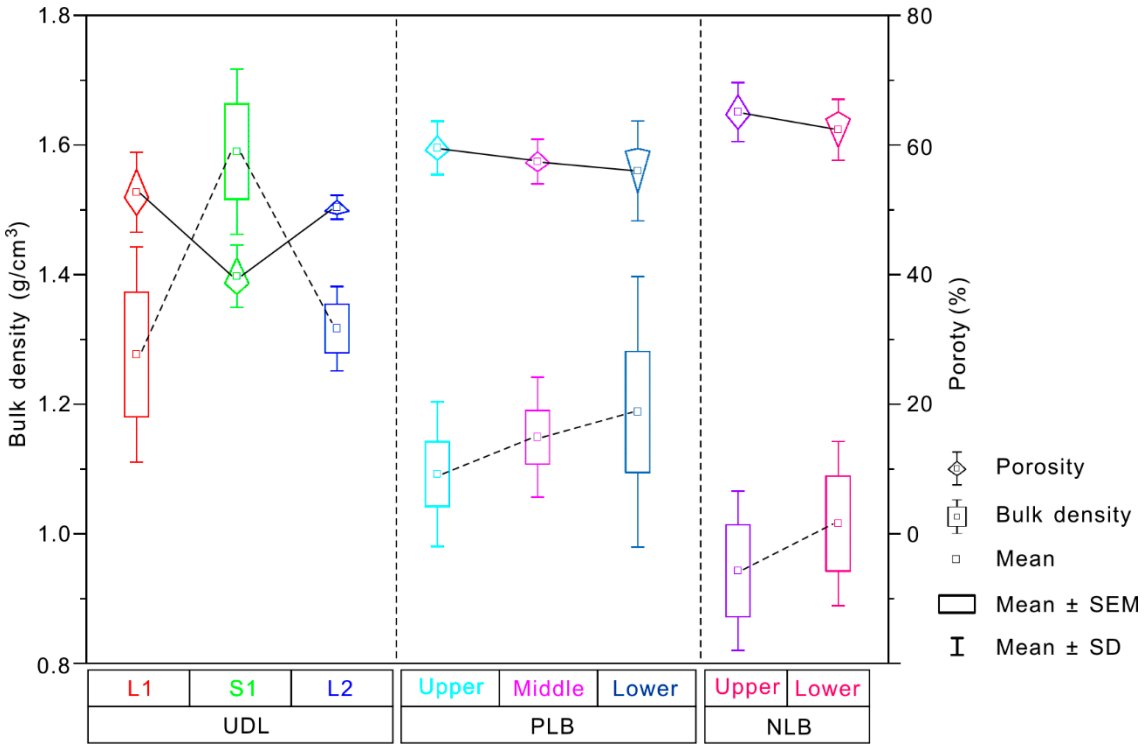

Figure 6. Comparison of the bulk density and porosity of the undisturbed loess (UDL), previous landslide body (PLB), and new landslide body (NLB). SEM is the standard error of mean. SD is the standard deviation.

5.4. Temporal Evolution of the Infiltration Rate in the Recent Landslide

To study the temporal evolution and the influence of physical crusts on the infiltration rate in the recent landslide, successive infiltration experiments were conducted in the upper part and lower part of the NLB on 14 March 2018 and 17 July 2018 (Table 2). The distance between the crusted and scalped experiment sites was 0.4–0.5 m. The results showed that the average IIR was dramatically greater on 26 October 2017 (no crust) than on 14 March 2018 (crusted) and 17 July 2018 (crusted) (Table 2), while the difference in the average infiltration rate between the crusted sites was small, exhibiting an insignificant decrease from 14 March 2018 to 17 July 2018 ($p = 0.794$) (Table 2). However, there was a significant decrease from 14 March 2018 to 17 July 2018 in the scalped sites ($p < 0.05$) (Table 2), and the results from both dates were greater in the scalped plots than in the crusted sites ($p < 0.05$) (Table 2).

Table 2. Infiltration rates on 26 October 2017, 14 March 2018, and 17 July 2018 for the new landslide body (NLB). SEM is the standard error of the mean.

	Without Crust (mm/min)		Crusted (mm/min)		Scalped (mm/min)	
	Mean	**SEM**	**Mean**	**SEM**	**Mean**	**SEM**
26 October 2017	855.4	89.4	—	—	—	—
14 March 2018	—	—	11.6 ^{a}	1.7	51.3 ^{b}	7.9
17 July 2018	—	—	10.9 ^{a}	0.7	29.7 ^{c}	8.2

Note. Different superscript letters within a row or a column indicate significant differences exist between the infiltration rate of crusted and scalped ($p < 0.05$) (e.g., a and b indicate significant differences between the infiltration rate of crusted and scalped). Same superscript letter within a column indicate no significant differences between the infiltration rate on different infiltration experiments ($p > 0.05$).

6. Discussion

6.1. The Reason for Spatial Differences in the Infiltration Rate

In this study, the infiltration experiment results showed that the average infiltration rate was dramatically highest in the NLB, intermediate in the PLB, and lowest in the UDL. As expected, the highest IIR occurred in the NLB, which can be attributed to the high degree of collapsibility of fragmented loess and the lack of obstruction by crusts on the soil surface [4,29,39]. The IIR value in the PLB was 4.4 times higher than that in the UDL, and we attributed this result to the loose structure of the disturbed loess and the weak cementation between soil particles, which is not easily restored to the level of UDL within a short time [37]. Furthermore, the recovery state and surface soil crusts can account for the spatial differences in the PLB. In the UDL, the infiltration rate was higher in the loess layers (L1 and L2) than in the paleosol layer (S1), which can be attributed to the loess having a lower bulk density and a higher porosity than the paleosol.

6.2. Role and Function of Physical Crusts in the Infiltration Rate in a Recent Landslide

The average IIR decreased sharply from 855.4 mm/min on 26 October 2017 (without crust), to 11.6 mm/min on 14 March 2018 (crusted) (Table 2). We attributed this decline to the appearance of physical crusts. On the other hand, the infiltration rate was significantly lower on 17 July 2018 than on 14 March 2018 on the scalped plots (Table 2), which can be attributed to the compaction effect related to the quality of the soil. The ecosystem processes of infiltration, surface runoff and erosion are influenced by the surface conditions of soil [40,41]. The infiltration rate is likely to be higher in areas without the obstruction of surface soil crusts [13,42,43], especially for disturbed soils. Given the way in which crusts affect the distribution of surface water, the effects of the crusts on the infiltration rate and variability on a recent landslide are unknown.

First, to better study the temporal evolution of infiltration on recent landslides, it is necessary to understand the formation mechanism and duration of physical crusts. Previous studies have assumed that raindrop impacts are the main driver of physical crust formation [44,45] and that the rainfall intensity influences the physical crust thickness. Simulated rainfall experiments have shown that the crust thickness slowly increases with increasing rainfall intensity [45,46]. However, researchers have different opinions on the duration of physical crust formation. Eldridge believed that this process requires one year in situations of suitable rainfall [29], while Bresson believed that a physical crust is likely to form after one or two rainfall and drying events [22]. In Han's study, the crusts formed rapidly under laboratory conditions (within one hour) [44]. Regardless, these researchers all agree that a physical crust can dramatically decrease the infiltration rate. In this study, data from successive investigations conducted on the NLB (Figure 7) suggested that physical crust formation requires four to five months and that the crust thickness increased slowly (Table 3). Data from the Baqiao meteorological station showed that one third of the days in January 2018 were snowy or rainy, with a mean daily temperature of −1 °C. Then, the temperature gradually increased from 12 February 2018. Therefore, because of the effects of heavy snowfall, rainfall and temperature increases, distinct physical crusts were found on 14 March 2018 (Figure 7b), and the crust thickness increased slowly from 0.5–1.5 mm (14 March 2018) to 1–2 mm (17 July 2018) (Table 3). Based on the effect of physical crusts on the infiltration rate, the results showed that the physical crusts were responsible for the initial rapid decrease in the infiltration rate; however, over longer time scales, the infiltration rate slowly decreased.

Table 3. Investigations and measurements of the physical crust thickness, physical parameters and recovery of vegetation on the new landslide body (NLB).

	Physical Crust Thickness (mm)	Bulk Density (g/cm^3)	Porosity (%)	Height of Grass (cm)
26 October 2017	No crust	0.8–1.2	57.1–69.8	No grass
14 March 2018	0.5–1.5	0.9–1.2	55.4–64.2	5–10
17 July 2018	1–2	1.0–1.3	45.5–57.2	50–120

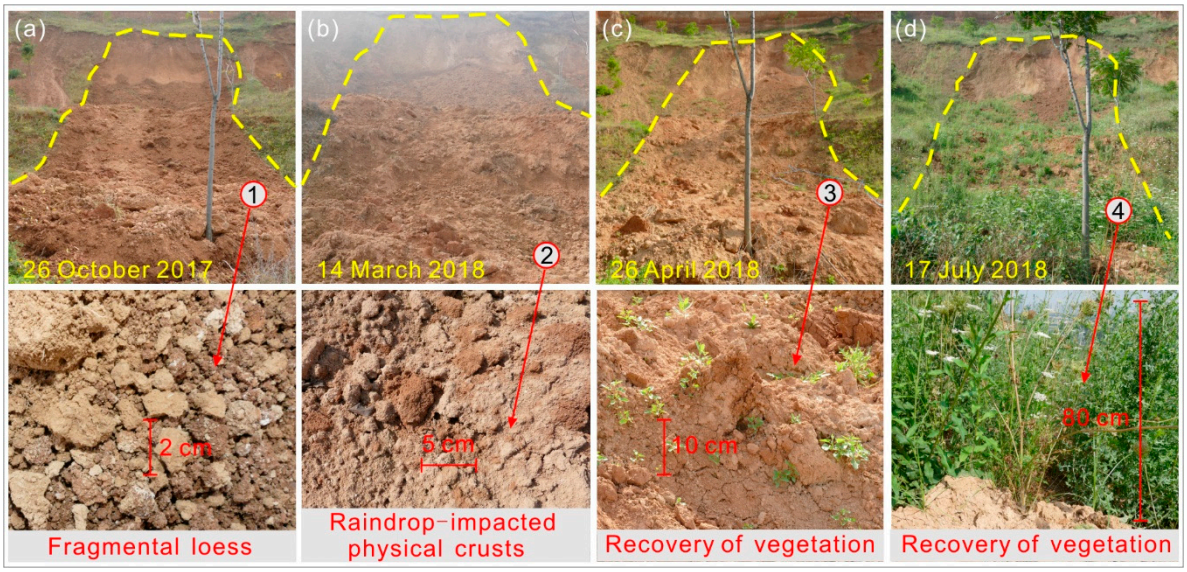

Figure 7. The recovery of the physical crusts and vegetation on the new landslide body (NLB). (**a**) Field investigation on 26 October 2017, (**b**) field investigation on 14 March 2018, (**c**) field investigation on 26 April 2018 and (**d**) field investigation on 17 July 2018. ①, ②, ③, and ④ show the features in (**a**), (**b**), (**c**), and (**d**), respectively.

6.3. Role and Function of Biological Crusts and Moss Crusts on a Landslide Body

Physical crusts, biological crusts, and moss crusts are the principal types of soil crusts. However, the duration of biological crust formation is much longer than that of physical crusts. In fact, the recovery of biological crusts requires 5 to 20 years [47], and other studies have suggested that biological crusts can form within 6 years on bare soil after shrub death [48]. Higher rainfall amounts will promote moss and lichen growth after the soil is stabilized by cyanobacteria [47]. Therefore, this slow growth process is the reason that no biological or moss crusts were found on the NLB in the recent investigation (17 July 2018) (Figure 7d). In contrast, physical crusts, biological crusts, and moss crusts were observed on the PLB, and the thicknesses of the crusts were 0.5–2 cm, 0.5–1 cm, and 2–3 cm, respectively. It is speculated that biological crusts can develop on disturbed soil within 5 to 7 years following landslide formation. Furthermore, there has long been a debate regarding whether biological crust formation decreases or increases the infiltration rate. The research of Warren [49] suggested that most biological crusts have a positive effect on infiltration according to 13 studies. This result may account for the higher infiltration rate in the PLB compared to that in the UDL.

6.4. The Temporal Evolution of the Infiltration Rate in a Recent Landslide

Loess failure can change the microstructure of the soil, further influencing its macroscopic geotechnical properties. Therefore, the interparticle cementation and shear strength of disturbed soil are lower than those of undisturbed soil [37,50]. In fact, these variations have a remarkable impact on infiltration. Therefore, loess landslides can cause the infiltration rate to significantly increase during

the one to three months after landslide formation because of the changes in the loess structure [51,52]. Due to the influences of the recovery state, rainfall, temperature, and microbial activities, moss crusts and biological crusts begin to form and gradually thicken within 5 to 20 years [28,29,53], causing the infiltration rate in recent landslides to decrease slowly [54]. According to the results of this study, more than 10 years may be required for the disturbed soil caused by a landslide to recover the same infiltration rate as UDL.

7. Conclusions

Our experiments revealed that the loess landslide process resulted in greatly increased infiltration, especially in a recent landslide. The average IIR in the NLB was approximately 200 times and 60 times higher than that in the UDL and PLB, respectively. Moreover, the infiltration capacity in the loess layer was slightly higher than that in the paleosol layer. Spatially, the infiltration rate in the PLB was highest in the upper part, intermediate in the middle part, and lowest in the lower part. Successive investigation and experiments conducted on the NLB revealed that the formation of raindrop-induced physical crusts caused the infiltration rate to rapidly decrease for four to five months, after which it slowly decreased. The results may decrease the risk of damage and offer suggestions when a landslide body needs to be used for industrial applications or as farmland.

Author Contributions: Conceptualization, Haijun Qiu; Methodology, Dongdong Yang; Sheng Hu; Mingming Cao; Software, Sheng Hu; Validation, Yanqian Pei; Formal Analysis, Yan Zhang; Investigation, Dongdong Yang; Yanqian Pei; Shuyue Ma; Zijing Liu; Data Curation, Zijing Liu; Writing-Original Draft Preparation, Dongdong Yang; Writing-Review & Editing, Haijun Qiu; Visualization, Dongdong Yang; Supervision, Haijun Qiu; Project Administration, Haijun Qiu; Funding Acquisition, Haijun Qiu. All authors have read and agreed to the published version of the manuscript.

Funding: This work was funded by the Second Tibetan Plateau Scientific Expedition and Research (STEP) program (Grant No. 2019QZKK0903), International Science & Technology Cooperation Program of China (Grant No. 2018YFE0100100), National Natural Science Foundation of China (Grant No. 41771539), China Postdoctoral Science Foundation (Grant No. 2019M663792), Strategic Priority Research Program of Chinese Academy of Sciences (Grant No. XDA 20030301), International Partnership Program of Chinese Academy of Sciences (Grant No. 131551KYSB20160002) and Key Laboratory of Degraded and Unused Land Consolidation Engineering of the Ministry of Natural Resources, China (Grant No. SXDJ2019-07).

Acknowledgments: The authors would like to thank Bin Tang and Weiqiang Guo for helping us during the landslide investigation.

Conflicts of Interest: The authors declare no conflict of interest.

References

1. Tu, X.B.; Kwong, A.K.L.; Dai, F.C.; Tham, L.G.; Min, H. Field monitoring of rainfall infiltration in a loess slope and analysis of failure mechanism of rainfall-induced landslides. *Eng. Geol.* **2009**, *105*, 134–150. [CrossRef]
2. Kong, Y.; Ruan, H.N.; Huang, X.F. Field testing of earth pressures in a large-scale natural loess slope. *KSCE J. Civ. Eng.* **2017**, *22*, 1–8. [CrossRef]
3. Liu, T.S. *Loess and Environment*; China Ocean Press: Beijing, China, 1985.
4. Ryashchenko, T.G.; Akulova, V.V.; Erbaeva, M.A. Loessial soils of Priangaria, Transbaikalia, Mongolia, and northwestern China. *Quat. Int.* **2008**, *179*, 90–95. [CrossRef]
5. Wang, J.J.; Liang, Y.; Zhang, H.P.; Wu, Y.; Lin, X. A loess landslide induced by excavation and rainfall. *Landslides* **2014**, *11*, 141–152. [CrossRef]
6. Qiu, H.J.; Cui, P.; Regmi, A.D.; Wang, Y.; Hu, S. Slope height and slope gradient controls on the loess slide size within different slip surfaces. *Phys. Geogr.* **2017**, *38*, 303–317. [CrossRef]
7. Zhuang, J.Q.; Peng, J.B. A coupled slope cutting-a prolonged rainfall-induced loess landslide: A 17 October 2011 case study. *Bull. Eng. Geol. Environ.* **2014**, *73*, 997–1011. [CrossRef]
8. Xu, X.Z.; Guo, W.Z.; Liu, Y.K.; Ma, J.Z.; Wang, W.L.; Zhang, H.W.; Gao, H. Landslides on the Loess Plateau of China: A latest statistics together with a close look. *Nat. Hazards* **2017**, *86*, 1393–1403. [CrossRef]
9. Zhang, X.; Li, P.; Li, Z.B.; Yu, G. Characteristics and formation mechanism of the July 25, 2013, Tianshui group-occurring geohazards. *Environ. Earth Sci.* **2017**, *76*, 219. [CrossRef]

10. Qiu, H.J.; Cui, P.; Regmi, A.D. Landslide distribution and size versus relative relief (Shaanxi Province, China). *Bull. Eng. Geol. Environ.* **2018**, *77*, 1331–1342. [CrossRef]
11. Zhang, F.; Wang, G. Effect of irrigation-induced densification on the post-failure behavior of loess flowslides occurring on the Heifangtai area, Gansu, China. *Eng. Geol.* **2018**, *236*, 111–118. [CrossRef]
12. Qiu, H.J.; Cui, P.; Hu, S. Size distribution and size of loess slides in response to slope height and slope gradient based on field survey data. *Geomat. Nat. Hazards Risk.* **2019**, *10*, 1443–1458. [CrossRef]
13. Lowery, B.; Hickey, W.J.; Arshad, M.A.; Lal, R. Soil Water Parameters and Soil Quality. In *Methods for Assessing Soil Quality*; Doran, J.W., Jones, A.J., Eds.; Segoe Rd: Madison, WI, USA, 1996; pp. 143–155.
14. Xu, L.; Qiao, X.; Wu, C.; Iqbal, J.; Dai, F. Causes of landslide recurrence in a loess platform with respect to hydrological processes. *Nat. Hazards* **2012**, *64*, 1657–1670. [CrossRef]
15. Zhou, Y.F.; Tham, L.G.; Yan, W.M.; Dai, F.C.; Xu, L. Laboratory study on soil behavior in loess slope subjected to infiltration. *Eng. Geol.* **2014**, *183*, 31–38. [CrossRef]
16. Leng, Y.; Peng, J.; Wang, Q.; Meng, Z.; Huang, W. A fluidized landslide occurred in the Loess Plateau: A study on loess landslide in South Jingyang tableland. *Eng. Geol.* **2017**, *236*, 129–136. [CrossRef]
17. Cogan, J.; Gratchev, I.; Wang, G. Rainfall-induced shallow landslides caused by ex-Tropical Cyclone Debbie, 31 March 2017. *Landslides* **2018**, *15*, 1215–1221. [CrossRef]
18. Derbyshire, E. Geological hazards in loess terrain, with particular reference to the loess regions of China. *Earth-Sci. Rev.* **2001**, *54*, 231–260. [CrossRef]
19. Qiu, H.J.; Regmi, A.D.; Cui, P. Size distribution of loess slides in relation to local slope height within different slope morphologies. *Catena* **2016**, *145*, 155–163. [CrossRef]
20. Qiu, H.J.; Cui, P.; Regmi, A.D. Influence of topography and volume on mobility of loess slides within different slip surfaces. *Catena* **2017**, *157*, 180–188. [CrossRef]
21. Zhang, F.; Huang, X. Trend and spatiotemporal distribution of fatal landslides triggered by non-seismic effects in China. *Landslides* **2018**, *15*, 1663–1674. [CrossRef]
22. Bresson, L.M.; Valentin, C. Soil Surface Crust Formation: Contribution of Micromorphology. In *Developments in Soil Science 22, Soil Micromorphology: Studies in Management and Genesis*; Ringrose-Voase, A.J., Humphreys, G.S., Eds.; Elsevier: Amsterdam, The Netherlands, 1994; pp. 737–762.
23. Casanova, M.; Messing, I.; Joel, A. Influence of aspect and slope gradient on hydraulic conductivity measured by tension infiltrometer. *Hydrol. Process.* **2000**, *14*, 155–164. [CrossRef]
24. Hu, W.; Shao, M.; Wang, Q.; Fan, J.; Horton, R. Temporal changes of soil hydraulic properties under different land uses. *Geoderma* **2009**, *149*, 355–366. [CrossRef]
25. Zhao, J.; Ma, Y.; Cao, J.; Wei, J.; Shao, T. Effect of Quaternary climatic change on modern hydrological systems in the southern Chinese Loess Plateau. *Environ. Earth Sci.* **2015**, *73*, 1161–1167. [CrossRef]
26. Van Asch, T.W.; Buma, J.; Van Beek, L.P.H. A view on some hydrological triggering systems in landslides. *Geomorphology* **1999**, *30*, 25–32. [CrossRef]
27. Wang, G.; Sassa, K. Pore-pressure generation and movement of rainfall-induced landslides: Effects of grain size and fine-particle content. *Eng. Geol.* **2003**, *69*, 109–125. [CrossRef]
28. Zaady, E.; Gutterman, Y.; Boeken, B. The germination of mucilaginous seeds of t Plantago coronopus, Reboudia pinnata, and t Carrichtera annua on cyanobacterial soil crust from the Negev Desert. *Plant Soil* **1997**, *190*, 247–252. [CrossRef]
29. Eldridge, D.J.; Zaady, E.; Shachak, M. Infiltration through three contrasting biological soil crusts in patterned landscapes in the Negev, Israel. *Catena* **2000**, *40*, 323–336. [CrossRef]
30. Qiu, H.J.; Cui, P.; Regmi, A.D. The effects of slope length and slope gradient on the size distributions of loess slides: Field observations and simulations. *Geomorphology* **2018**, *300*, 69–76. [CrossRef]
31. Zhao, J.B.; Tian, J.S.; Jun, J.N. Permeability and water-bearing conditions of loess in Bailu tableland in the eastern suburbs of Xi'an. *Geogr. Res.* **2009**, *28*, 1188–1196.
32. Cheng, Q.; Chen, X.; Chen, X.; Zhang, Z.; Ling, M. Water infiltration underneath single-ring permeameters and hydraulic conductivity determination. *J. Hydrol.* **2011**, *398*, 135–143. [CrossRef]
33. Bagarello, V.; Prima, S.D.; Iovino, M.; Provenzano, G. Estimating field-saturated soil hydraulic conductivity by a simplified beerkan infiltration experiment. *Hydrol. Process.* **2014**, *28*, 1095–1103. [CrossRef]
34. Hu, G.T.; Yang, W.Y. *Engineering Geology*; Geology Press: Beijing, China, 1987; pp. 26–30.
35. Belnap, J. The potential roles of biological soil crusts in dryland hydrologic cycles. *Hydrol. Process.* **2006**, *20*, 3159–3178. [CrossRef]

36. Saxton, K.E.; Rawls, W.J. Soil water characteristic estimates by texture and organic matter for hydrologic solutions. *Soil Sci. Soc. Am. J.* **2006**, *70*, 1569–1578. [CrossRef]
37. Strudley, M.W.; Green, T.R.; Ascough, J.C. Tillage effects on soil hydraulic properties in space and time: State of the science. *Soil Tillage Res.* **2008**, *99*, 4–48. [CrossRef]
38. Mueller, L.; Kay, B.D.; Deen, B.; Hu, C.; Zhang, Y.; Wolff, M.; Schindler, U. Visual assessment of soil structure: Part II. Implications of tillage, rotation and traffic on sites in Canada, China and Germany. *Soil Tillage Res.* **2009**, *103*, 188–196. [CrossRef]
39. Celik, I. Land-use effects on organic matter and physical properties of soil in a southern Mediterranean highland of Turkey. *Soil Tillage Res.* **2005**, *83*, 270–277. [CrossRef]
40. Badorreck, A.; Gerke, H.H.; Hüttl, R.F. Morphology of physical soil crusts and infiltration patterns in an artificial catchment. *Soil Tillage Res.* **2013**, *129*, 1–8. [CrossRef]
41. Błońska, E.; Lasota, J.; Zwydak, M.; Klamerus-Iwan, A.; Gołąb, J. Restoration of forest soil and vegetation 15 years after landslides in a lower zone of mountains in temperate climates. *Ecol. Eng.* **2016**, *97*, 503–515. [CrossRef]
42. Langhans, T.M.; Storm, C.; Schwabe, A. Regeneration processes of biological soil crusts, macro-cryptogams and vascular plant species after fine-scale disturbance in a temperate region: Recolonization or successional replacement? *Flora* **2010**, *205*, 46–60. [CrossRef]
43. Wang, H.; Zhang, G.H.; Liu, F.; Geng, R.; Wang, L.J. Temporal variations in infiltration properties of biological crusts covered soils on the Loess Plateau of China. *Catena* **2017**, *159*, 115–125. [CrossRef]
44. Han, Y.; Fan, Y.; Xin, Z.; Wang, L.; Cai, Q.; Wang, X. Effects of wetting rate and simulated rain duration on soil crust formation of red loam. *Environ. Earth Sci.* **2016**, *75*, 149. [CrossRef]
45. Vaezi, A.R.; Ahmadi, M.; Cerdà, A. Contribution of raindrop impact to the change of soil physical properties and water erosion under semi-arid rainfalls. *Sci. Total Environ.* **2017**, *583*, 382–392. [CrossRef] [PubMed]
46. Lu, J.; Zheng, F.; Li, G.; Bian, F.; An, J. The effects of raindrop impact and runoff detachment on hillslope soil erosion and soil aggregate loss in the Mollisol region of Northeast China. *Soil Tillage Res.* **2016**, *161*, 79–85. [CrossRef]
47. Belnap, J.; Lange, O.L. *Biological Soil Crusts; Structure, Function, and Management*; Springer: Berlin, Germany, 2001; p. 503.
48. Nejidat, A.; Potrafka, R.M.; Zaady, E. Successional biocrust stages on dead shrub soil mounds after severe drought: Effect of micro-geomorphology on microbial community structure and ecosystem recovery. *Soil Biol. Biochem.* **2016**, *103*, 213–220. [CrossRef]
49. Warren, S.D. Synopsis: Influence of Biological Soil Crusts on Arid Land Hydrology and Soil Stability. In *Biological Soil Crusts: Structure, Function, and Management*; Springer: Berlin/Heidelberg, Germany, 2001; pp. 349–360.
50. Luo, H.; Wu, F.; Chang, J.; Xu, J. Microstructural constraints on geotechnical properties of Malan Loess: A case study from Zhaojiaan landslide in Shaanxi province, China. *Eng. Geol.* **2018**, *236*, 60–69. [CrossRef]
51. Bo, X.; Wang, Q.H.; Zhao, Y.G.; Shao, M.A. Artificial culture of biological soil crusts and its effects on overland flow and infiltration under simulated rainfall. *Appl. Soil Ecol.* **2011**, *48*, 11–17.
52. Qiu, H.J.; Cui, Y.F.; Pei, Y.Q.; Yang, D.D.; Hu, S.; Wang, X.G.; Ma, S.Y. Temporal patterns of nonseismically triggered landslides in Shaanxi Province, China. *Catena* **2019**. [CrossRef]
53. Zaady, E.; Groffman, P.; Shachak, M. Nitrogen fixation in macro-and microphytic patches in the Negev desert. *Soil Biol. Biochem.* **1998**, *30*, 449–454. [CrossRef]
54. Stokes, A.; Sotir, R.; Chen, W.; Ghestem, M. Soil bio-and eco-engineering in China: Past experience and future priorities. *Ecol. Eng.* **2010**, *36*, 247–257. [CrossRef]